

CHEMISTRY

A European Journal

A Journal of



Accepted Article

Title: Controlled Pyrolysis of Ni-MOF-74 as a Promising Precursor for the Creation of Highly Active Ni Nanocatalysts in Size-selective Hydrogenation

Authors: Kazuki Nakatsuka, Takeharu Yoshii, Yasutaka Kuwahara, Kohsuke Mori, and Hiromi Yamashita

This manuscript has been accepted after peer review and appears as an Accepted Article online prior to editing, proofing, and formal publication of the final Version of Record (VoR). This work is currently citable by using the Digital Object Identifier (DOI) given below. The VoR will be published online in Early View as soon as possible and may be different to this Accepted Article as a result of editing. Readers should obtain the VoR from the journal website shown below when it is published to ensure accuracy of information. The authors are responsible for the content of this Accepted Article.

To be cited as: *Chem. Eur. J.* 10.1002/chem.201704341

Link to VoR: <http://dx.doi.org/10.1002/chem.201704341>

Supported by
ACES

WILEY-VCH

FULL PAPER

Controlled Pyrolysis of Ni-MOF-74 as a Promising Precursor for the Creation of Highly Active Ni Nanocatalysts in Size-selective Hydrogenation

Kazuki Nakatsuka,^[a] Takeharu Yoshii,^[a] Yasutaka Kuwahara,^[a, b] Kohsuke Mori,^[a, b, c] and Hiromi Yamashita*^[a, b]

Abstract: Metal organic frameworks (MOFs) are a class of porous organic-inorganic crystalline materials that have attracted much attention as H₂ storage, and catalytic supports. In this paper, the synthesis of highly-dispersed Ni nanoparticles (NPs) for the hydrogenation of olefins was achieved by employing Ni-MOF-74 as precursor. Investigations of the structural transformation of Ni species derived from Ni-MOF-74 during the heat treatment were conducted. The transformation was monitored in detail by a combination of XRD, *in-situ* XAFS, and XPS measurements. Ni NPs prepared from Ni-MOF-74 were easily reduced by the generation of reducing gases accompanied by the decomposition of Ni-MOF-74 structures during heat treatment at over 300 °C under N₂ flow. Ni-MOF-74-300 heat treated at 300 °C exhibited the highest activity for the hydrogenation of 1-octene due to efficient suppression of excess agglomeration of Ni species during heat treatment. Moreover, Ni-MOF-74-300 showed not only high activity for the hydrogenation of olefins but also high size-selectivity because of the selective formation of Ni NPs covered by MOFs and the MOF-derived carbonaceous layer.

19 Introduction

Heterogeneous catalysts are essential materials in the industrial manufacturing of many fine chemicals due to their recyclability.^[1] In order to synthesize highly active heterogeneous catalysts, various approaches, such as controlling the shape of metal NPs,^[2-6] utilization of the synergy effect between metal NPs and catalyst supports^[7-8], and alloying with second and third metals^[9-11], have been widely reported over several decades. However, the preparation of catalysts for size-selective hydrogenation of olefins with different molecular sizes is still a difficult problem. The most common approach to achieve size-selective catalysis is the fabrication of core-shell type catalysts with molecular sieving

properties to avoid the diffusion of huge molecules and/or poisoning of particular active sites to inhibit excess hydrogenation^[12-14]. However, such catalysts frequently suffer from lower reaction rates than conventional catalysts for selective hydrogenation. In this context, the preparation of heterogeneous catalysts that can simultaneously achieve both high activity and size-selectivity remains to be solved.

Metal organic frameworks (MOFs) consisting of metal clusters and organic bridging ligands have received much attention in a large number of applications such as gas storage/separation^[15-18], biomedical imaging^[19], drug delivery^[20-22], sensing^[23], and catalytic supports^[24-27] owing to their high porosity and tenability. MOFs have recently been utilized as efficient heterogeneous catalysts with molecular sieving properties owing to their separation ability. This ability is derived from their well-defined microporous structure, which enables separation of many kinds of molecules of different sizes. For example, core-shell type and hollow type MOF catalysts (Pt NPs@MIL-101, Pd NPs@void@ZIF-8, etc.), which consist of finely structured metal NPs incorporated into a MOF shell, were previously reported for size-selective hydrogenation^[28-31]. In addition, the apical metal coordination sites in the MOF networks were proven to act as catalytic active sites for various organic reactions, such as N-arylation (MOF-199, Cu-based MOF)^[32] and alkene oxidation (MIL-101(Fe), Fe-based MOF)^[33]. Our previous work also demonstrated that the Zr clusters in the framework of UiO-66 functioned as Lewis basic sites, which promoted the hydrogen transfer reaction of biomass-derived esters (e.g., methyl levulinate)^[34]. Unfortunately, most metal species in the frameworks of MOFs are coordinated with the organic linkers, resulting in a limited number of metal species that can be involved in catalytic reactions, thereby restricting the extensive application of MOFs as heterogeneous catalysts.

The preparation of metal NPs by employing MOFs as precursor materials by simple pyrolysis under inert gas has emerged recently in the electrocatalytic field^[35-42]. In this method, to construct MOFs, metal clusters serve as the metal precursor while organic linkers are the source of carbon supports. The metal species emerging from the frameworks of MOFs during thermal decomposition are accessible by substrate molecules and can act as active sites for the catalytic reaction^[41, 43-45]. However, the deconstruction of the MOF structure means the loss of the molecular sieving property, which accordingly results in the decrease in size-selectivity. Considering these reports, the design of promising active species with suitable catalytic structures that

[a] K. Nakatsuka, T. Yoshii, Dr. Y. Kuwahara, Prof. Dr. K. Mori, Prof. Dr. H. Yamashita

Graduate School of Engineering,
Osaka University.

2-1 Yamadaoka, Suita, Osaka 565-0871, Japan.

E-mail: yamashita@mat.eng.osaka-u.ac.jp (H. Yamashita)

[b] Dr. Y. Kuwahara, Prof. Dr. K. Mori, Prof. Dr. H. Yamashita
Elements Strategy Initiative for Catalysts & Batteries (ESICB)
Kyoto University

Katsura, Kyoto 615-8520, Japan.

[c] Prof. Dr. K. Mori

JST, PRESTO

4-1-8 Honcho, Kawaguchi, Saitama 332-0012, Japan.

Supporting information of this article can be found under :
<http://dx.doi.org/10.1002/0000000>.

FULL PAPER

exhibit high catalytic activity as well as selectivity by the structural transformation of MOF materials is of great interest.

In this paper, we report the successful preparation of highly active and size-selective Ni-based nanocatalysts derived from Ni-MOF-74 by heat treatment at low temperature, and conduct detailed investigation of the structural transformations during the heat treatment. The structures and properties of prepared materials including catalytic active sites are investigated by combination of various techniques, such as XRD, in situ XAFS, SEM, HAADF-STEM, XPS, and N_2 adsorption/desorption measurements. The ordered porosity of Ni-MOF-74 decomposes at around 300 °C to form Ni NPs with the release of reducing gases such as CO_2 and CH_4 , which reduce Ni^{2+} derived from the Ni cluster in Ni-MOF-74 to Ni^0 metal. The created Ni NPs are incorporated within the deformed MOF structure and show unique catalytic properties in the hydrogenation of olefins, which are significantly higher than those of as-synthesized Ni-MOF-74 without heat treatment and conventional Ni based catalysts such as Ni NPs supported on activated carbon (Ni/AC).

20 Results and Discussion

21 Characterization of the structure of Ni-MOF-74-T

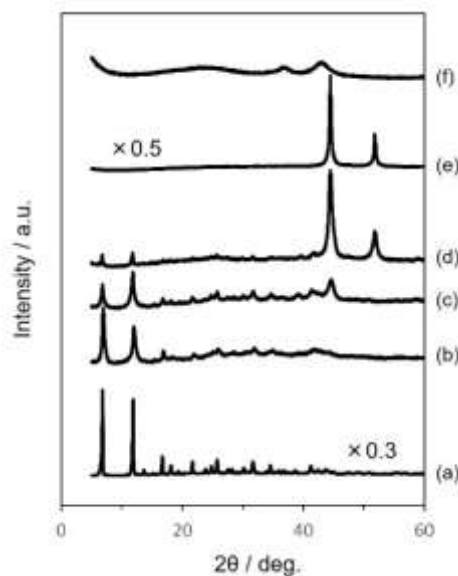


Figure 1. XRD patterns of (a) – (e) Ni-MOF-74-T and (f) Ni/AC-300. Heat treatment temperature T: (a) untreated, (b) 250 °C, (c) 300 °C, (d) 400 °C and (e) 600 °C.

The XRD patterns of Ni-MOF-74 (Figure 1) show two characteristic sharp peaks at around $2\theta = 6.8^\circ$ and 11.7° that coincide with those of typical Ni-MOF-74^[46], indicating successful formation of Ni-MOF-74. The intensities of these peaks decrease with increasing heat treatment temperature, and is accompanied by the appearance of new two peaks at around $2\theta = 44.4^\circ$ and 51.8° corresponding to Ni metals in the Ni-MOF-74-T samples

> 300 °C^[47]. These results indicate the structural transformation is initiated at around 300 °C and the structure of Ni-MOF-74 is continuously degraded during the heat treatment process. On the other hand, Ni/AC-300 shows two peaks at around $2\theta = 37.4^\circ$ and 43.3° corresponding to NiO instead of the Ni metal species^[48], which indicates that the decomposition process of Ni-MOF-74 during heat treatment for the formation of Ni NPs is different from that of Ni/AC-300. These Ni species are likely to be oxidized by the oxygens of functional groups abundantly present on the carbon support surface.

In order to investigate the state of Ni species in Ni-MOF-74 during the heat treatment, the decomposition profiles of the Ni-MOF-74 were monitored by TPD (Figure S2). In the case of Ni-MOF-74, the peaks corresponding to H_2 ($m/z = 2$) and CH_4 ($m/z = 16$) gases were clearly observed at around 300 °C and 450 °C with simultaneous release of CO ($m/z = 28$) and CO_2 ($m/z = 44$). On the other hand, these reducing gas peaks are not observed in the sample of $Ni(NO_3)_2$ supported on AC as the precursor of Ni/AC-300. These reducing gases reacted with the Ni clusters incorporated in Ni-MOF-74 to form Ni metal during the heat treatment process, which is the main cause for the emergence of Ni metal in the Ni-MOF-74-T samples ($T > 300^\circ C$).

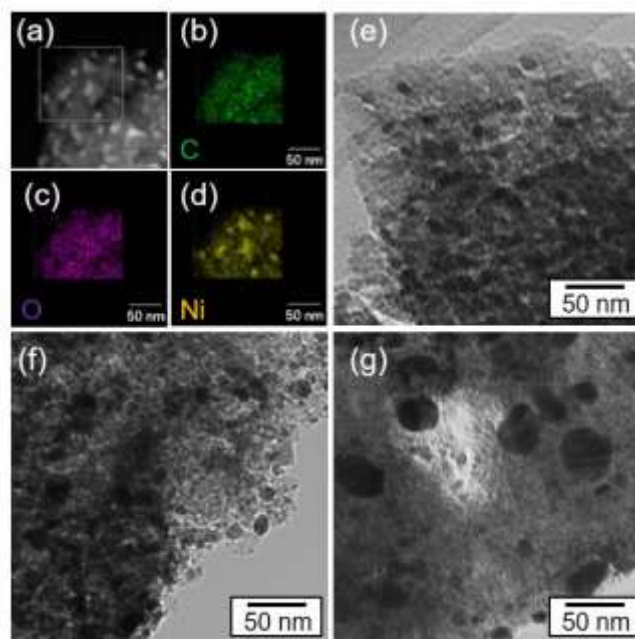


Figure 2. (a) HAADF-STEM images, (b) – (d) EDS elemental mapping results ((b) C, (c) Ni, (d) O) and (e) TEM image of Ni-MOF-74-300 and TEM images of Ni/AC-300 (f) before and (g) after the hydrogen reduction.

The crystal shapes of Ni-MOF-74-T samples were confirmed by FE-SEM observations (Figure S3). The as-synthesized Ni-MOF-74 sample before heat treatment exhibited the inherent rose-like morphology representing high crystallinity, which was retained in Ni-MOF-74-250 (Figure S3 (b)). However, some new mesopores appeared on the crystal surface of Ni-MOF-74-300

FULL PAPER

1 (marked with red circles) although it also retained a similar morphology (Figure S3 (c), (d)). Moreover, the edge of the crystal was slightly damaged, indicating that crystallinity was reduced with increasing heat treatment temperature. Significant changes in the crystal were confirmed in the samples heat-treated at over 400 °C, in which the exterior rose-like shape was configured with millions of small particles (Figure S3 (f), (h)). The Ni-MOF-74 crystal was almost completely decomposed by the heat treatment at 600 °C. Based on these results, Ni-MOF-74 is likely decomposed at a temperature between 300 and 400 °C.

11 A high-angle annular dark-field scanning transmission electron microscopy (HAADF-STEM), energy dispersive X-ray spectroscopy (EDS) mapping and transmission electron microscopy (TEM) image of Ni-MOF-74-300 and TEM images of Ni/AC-300 before and after hydrogen reduction were obtained to check the diameter of Ni NPs in the prepared samples (Figure 2). Highly-dispersed Ni NPs with an average diameter of 11.3 nm were confirmed throughout the observation area in Ni-MOF-74-300. Moreover, the number of Ni NPs exposed on the surface of MOF is significantly small, indicating the Ni NPs are selectively formed inside of Ni-MOF-74. The elemental distribution indicated that the Ni species in Ni-MOF-74-300 were reduced completely and present as Ni metal species. In addition, Ni atoms were distributed throughout both NPs and support, indicating Ni species constituted not only Ni NPs but also the frameworks of Ni-MOF-74. On the other hand, in TEM images of Ni/AC-300, an increase in the average diameter of Ni NPs by aggregation was confirmed by observations before (diameter of ca. 13.6 nm) and after (diameter of ca. 25.6 nm) hydrogen reduction pretreatment. The reduction of Ni species in Ni/AC-300 requires a higher temperature (at least 400 °C) than that required for Ni-MOF-74-T (200 °C) due to the absence of reducing gases during the heat treatment process, which is supported by TPD results. Hydrogen reduction at high temperature causes the aggregation of Ni species, resulting in the formation of Ni NPs with larger particle sizes. This is less effective for the hydrogenation reaction as will be discussed later.

38 In prepared samples, there is a possibility of the existence of porous structures with various pore diameters, such as micropores, mesopores and macropores. This was analyzed by applying Saito-Foley (SF) plot, Barrett-Joyner-Halenda (BJH) plot and Brunauer-Emmett-Teller (BET) methods (Figure 3, Table 1). In Figure 3 (a), the typical type I isotherms were observed in Ni-MOF-74, which is characteristic of MOF-74. For the relative pressure at around 0.0, the isotherm shows a sharp increase in the adsorbed N₂ attributed to the micropores. The average diameter of the microporous structure calculated from the SF plot is 0.59 nm (Figure 3 (b)) and the BET surface area and pore volume were estimated to be 1254 m²/g and 0.51 cm³/g (Table 1), respectively. These characteristics were similar to those found in previous works, indicating the successful synthesis of Ni-MOF-74. The shape of the isotherms and the average diameter of the microporous structure in Ni-MOF-74 were maintained even after thermal treatment at 250 °C, though the surface area and pore

volume calculated by the BET method were slightly decreased (884 m²/g and 0.45 cm³/g, respectively). A noticeable structural change occurred in Ni-MOF-74-300, in which a characteristic hysteresis for the type IV isotherm was clearly observed, indicating the formation of a mesoporous structure while retaining microporous structures derived from Ni-MOF-74. Therefore, SF plot and BJH plot were employed in order to estimate both micropores and mesopores for Ni-MOF-74-300. As can be seen in Figure 3 (B), (C), both distributions of pore diameters calculated by the SF plot and the BJH method clearly shows a peak (0.58 nm for SF plot and 10.2 nm for BJH plot), which correspond to micropores and mesopores, respectively. For Ni-MOF-74-400, the peak intensity for the distribution of microporous structures decreases and the diameter of the mesopores was expanded (32.6 nm), suggesting a further disruption of the Ni-MOF-74 structure. No micropores were confirmed in the sample of Ni-MOF-74-600 and the surface area was drastically decreased (124 m²/g). These results agreed well with the results of both XRD analysis and FE-SEM observations. Further analysis of the porous structure was carried out by using the α_s plot (Figure S4, Table S1). The tendency obtained from the α_s plot was similar to those mentioned above.

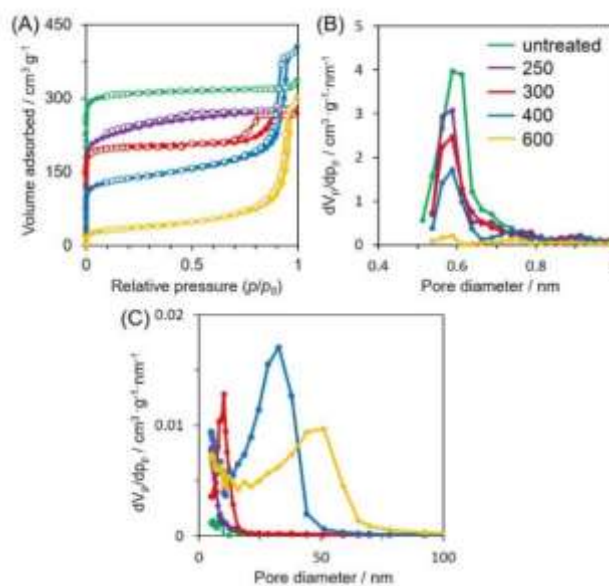
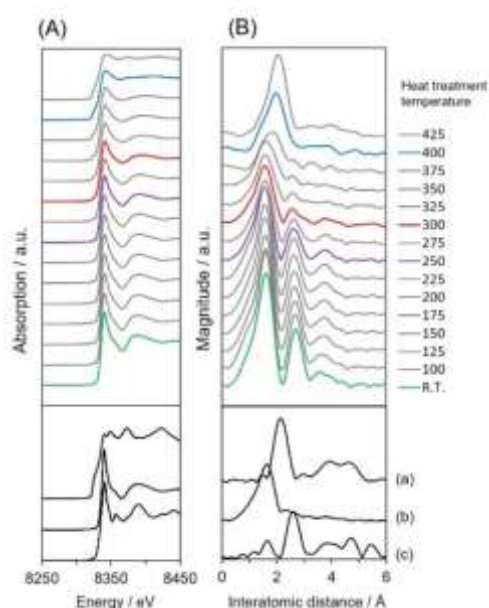


Figure 3. (A) N₂ adsorption/desorption isotherms, (B) SF plots and (C) BJH plots of Ni-MOF-74-T. Heat treatment temperature T : untreated, 250 °C, 300 °C, 400 °C and 600 °C. Open symbol: adsorption isotherms, closed symbol: desorption isotherms.

FULL PAPER

1 **Table 1.** Characteristics of Ni-MOF-74-T and Ni/AC-300 calculated by various
 2 methods. Heat treatment temperature T: (a) untreated, (b) 250 °C, (c) 300 °C,
 3 (d) 400 °C and (e) 600 °C.



4 **Figure 4.** Ni K-edge in-situ (A) XANES spectra and (B) FT-EXAFS spectra of
 5 (upper) Ni-MOF-74 during heat treatment under He atmosphere and reference
 6 samples. (a) Ni foil, (b) Ni(NO₃)₂, (c) NiO.

7 In order to investigate the continuous structural transformation
 8 of the active site during the heat treatment, *in situ* X-ray
 9 adsorption fine structure (XAFS) measurements were carried out
 10 from room temperature to 400 °C. Figure 4 shows the Ni K-edge
 11 X-ray absorption near-edge structure (XANES) and Fourier
 12 transformation of the extended X-ray absorption fine structure
 13 (FT-EXAFS) spectra of Ni-MOF-74-T with reference samples. In
 14 the XANES spectra, the shape of Ni-MOF-74 before heat
 15 treatment was similar to that of NiO and Ni(NO₃)₂, indicating Ni
 16 species in the Ni-MOF-74 network were present as Ni²⁺ ions.
 17 The FT-EXAFS spectrum for Ni-MOF-74 showed a strong
 18 absorption peak at around 1.7 Å, which was derived from the
 19 Ni-O bonds in the Ni cluster, and a second peak at around 2.7 Å
 20 attributed to neighboring Ni atoms (Ni-(O)-Ni bond). The
 21 transformation of the Ni-MOF-74 sample was confirmed at around
 22 375 °C in the FT-EXAFS spectra, in which the intensity of the first
 23 peak at around 1.7 Å decreased, indicating the decomposition of
 24 the Ni-MOF-74 structure accompanied by the formation of small
 25 Ni metal NPs. In the same temperature range, the absorption
 26 peak intensity of the XANES spectra at around 8835 eV
 27 decreases with increasing temperature. The shape of this peak
 28 similar to that of Ni foil. In addition, a new peak assigned to
 29 contiguous Ni-Ni bonds indicating the formation of Ni NPs was
 30 observed at around 2.2 Å, of which the intensity gradually
 31 increased accompanied by the disappearance of the first peak.

The Ni species in this range exists as a mixture of Ni cluster in Ni-MOF-74 and Ni NPs. Finally, it is estimated that the main peak position of Ni-MOF-74 heated at more than 425 °C is coincide with

Sample	SF plot	BJH plot	BET plot	
	$d_{SF,micro}^a$ [nm]	$d_{BJH,meso}^b$ [nm]	a_{BET}^c [m ² ·g ⁻¹]	V_{BET}^c [cm ³ ·g ⁻¹]
Ni-MOF-74	0.60	-	1254	0.51
Ni-MOF-74-250	0.58	-	884	0.45
Ni-MOF-74-300	0.58	10.2	809	0.42
Ni-MOF-74-400	0.58	32.6	506	0.62
Ni-MOF-74-600	-	51.1	124	0.46
Ni/AC-300	0.56	-	608	0.28

^a Diameter of micro pores calculated from SF plot.

^b Diameter of meso pores calculated from BJH plot.

^c Surface area and total pore volume calculated by BET method.

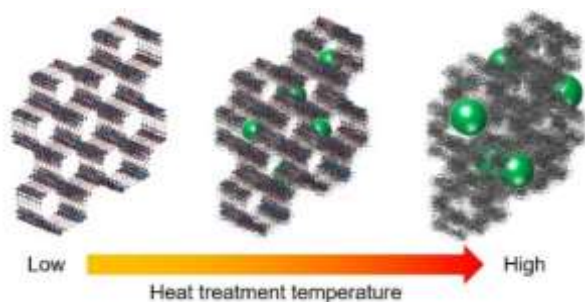
35 that of Ni foil, while the main peak position of Ni-MOF-74 heated
 36 at 425 °C is shown at lower interatomic distance. This result is
 37 well consistent with the results obtained by XRD, FE-SEM, and
 38 N₂ adsorption/desorption measurements.

39 The oxidation state and the electronic state of Ni species in
 40 the prepared samples were investigated by X-ray photoelectron
 41 spectroscopy (XPS). Figure 5 displays the Ni 2p_{3/2} XPS spectra
 42 of the series of Ni-MOF-74-T samples as well as Ni/AC-300 as a
 43 reference sample. As can be seen in Ni/AC-300, three peaks were
 44 observed at around 853.7 eV, 856.6 eV and 861.1 eV, which
 45 correspond to the NiO state, Ni²⁺ ionic state and Ni satellite peaks,
 46 respectively.^[51] From this result, Ni species in Ni/AC-300 existed
 47 in the NiO state, which supports the XRD results. Ni-MOF-74
 48 before heat treatment showed two distinct peaks at around 857.8
 49 eV and 862.4 eV, indicating that Ni species in Ni-MOF-74 existed
 50 as Ni²⁺ ions in the Ni cluster.^[52-53] No noticeable change was
 51 observed in the spectra of Ni-MOF-74-250 and Ni-MOF-74-300.
 52 The structural transformation was confirmed in Ni-MOF-74-400,
 53 in which the new peaks derived from Ni metal species appeared,
 54 and their intensities increased with increasing heat treatment
 55 temperature. However, these results for Ni-MOF-74-300 disagree
 56 with the results of XRD, TPD and XAFS in terms of the absence
 57 of Ni metal species. To investigate this anomaly, etching with ion
 58 guns was carried out for Ni-MOF-74-300. After 20 seconds of
 59 etching, a new peak was clearly observed at around 853.8 eV,
 60 indicating the appearance of Ni metal species on the surface of
 61 the Ni-MOF-74-300. These results suggest that the Ni NPs in the
 62 Ni-MOF-74-T are present inside Ni-MOF-74 crystals, resulting in
 63 the formation of a core-shell like structure. Moreover, the Ni⁰ and
 64 Ni²⁺ contents in Ni-MOF-74-300 sample were estimated to be 63
 65 and 37 %, respectively. This result suggests that ca. 60 % of Ni
 66 species in the Ni-MOF-74 seems to be decomposed during heat
 67 treatment at 300 °C accompanied with the formation of Ni NPs.

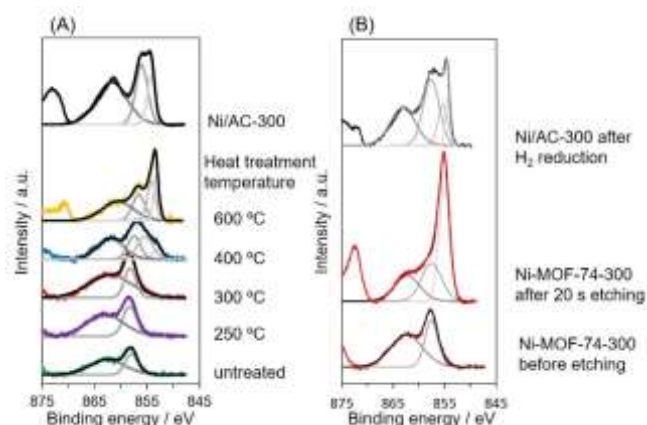
The Ni 2p_{3/2} peak position attributable to Ni metal species in Ni-MOF-74-300 (853.8 eV) is 1.0 eV energy-shifted from that of pure Ni metal (852.8 eV). The degree of this shift is slightly larger than that of Ni metallic species in Ni/AC-300 reduced by hydrogen at 400 °C (853.3 eV). Based on these results, the Ni species in Ni-MOF-74-300 are electronically more deficient compared to those

FULL PAPER

1 in Ni/AC-300 due to the stronger interaction between Ni species
 2 and carbonaceous species derived from Ni-MOF-74. In our
 3 previous work, the Co species prepared from Co(salen) complex
 4 supported onto AC also yielded electron-deficient Co species
 5 after heat treatment at 400 °C in an inert gas atmosphere, which
 6 suggests that metal species supported on carbon materials tend
 7 to become electronically deficient^[54-56]. Considering the results of
 8 XPS in both the previous work and this work, the contact area
 9 between Ni species and carbonaceous species in Ni-MOF-74-300
 10 is larger than that in Ni/AC-300. The obtained Ni-MOF-74-300
 11 likely has a core-shell like structure that consists of a Ni NPs core
 12 and a carbon/Ni-MOF-74 composite shell, which can be
 13 described as Ni NPs@carbon/Ni-MOF-74 (Scheme 1). In order to
 14 investigate effects of hydrogen reduction before catalytic
 15 reactions to the oxidation state of Ni species, XPS analysis of Ni
 16 MOF-74-300 before and after hydrogen reduction are carried out.
 17 In the results of XPS spectra, no changes are observed between
 18 before and after hydrogen reduction, which indicates that the Ni
 19 species in Ni-MOF-74 cannot be reduced by hydrogen reduction
 20 pretreatment prior to the reaction test (Fig S5).



24
 25 **Scheme 1.** Schematic illustration of the structural transformation of the Ni-MOF-74
 26 during the heat treatment.

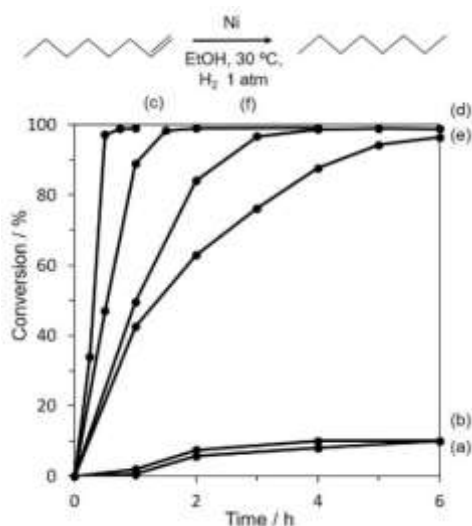


27
 28
 29 **Figure 5.** Ni 2p_{3/2} XPS spectra of (A) Ni-MOF-74-T and Ni/AC-300, and (B) Ni-MOF-74-300 before and after 20s etching and Ni/AC-300 after hydrogen reduction.

33 Catalytic test

34 To investigate the relationship between the structure and
 35 activities of the prepared Ni-MOF-74-T catalysts, the
 36 hydrogenation of olefins was carried out as a model reaction.
 37 Time courses using 1-octene as a substrate over the series of Ni-
 38 MOF-74-T are shown in Figure 6. Ni-MOF-74, Ni-MOF-74-250,
 39 and Ni/AC-300 (not shown) showed low activities, which indicates
 40 that Ni species in the frameworks and NiO are extremely low
 41 activity for this reaction (Figure 6 (a), (b)). On the other hand, Ni-
 42 MOF-74-300, Ni-MOF-74-400 and Ni-MOF-74-600 showed
 43 activities for this reaction as a result of Ni⁰ species reduced by the
 44 gases produced during the heat treatment process. Ni-MOF-74-
 45 300 exhibited the highest activity among the prepared samples,
 46 with 97% conversion of 1-octene after 0.5 h of reaction, which was
 47 twice that of Ni/AC-300 reduced with hydrogen at 400 °C (44%
 48 conversion after 0.5 h). Moreover, from the elemental mapping of
 49 Ni, Ni species in the Ni-MOF-74-300 also formed Ni-MOF-74
 50 frameworks, which suggests the actual amount of Ni NPs involved
 51 in the hydrogenation in Ni-MOF-74-300 is lower than that in
 52 Ni/AC-300. Considering these data, highly active Ni NPs were
 53 created in Ni-MOF-74-300 due to the formation of highly
 54 dispersed and electron-deficient Ni NPs, which is supported by
 55 the results of HAADF-STEM images and XPS spectra. The
 56 activities of Ni-MOF-74-400 and -600 gradually decreased with
 57 increasing heat treatment temperature, due to the excessive
 58 aggregation of Ni NPs caused by heat treatment at high
 59 temperatures.

FULL PAPER



1

2

3

4

Figure 6. Time course in the hydrogenation of 1-octene over Ni-MOF-74-T (a) untreated, (b) 250, (c) 300, (d) 400 and (e) 600 and (f) Ni/AC-300. Reaction condition: catalyst (10 mg), 1-octene (1 mmol), EtOH (10 mL) at 30 °C.

5

6

7

8

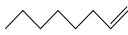
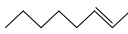
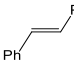

9

Table 2 summarizes the scope of substrates for the hydrogenation of olefins over Ni-MOF-74-T and Ni/AC-300. When substrates of smaller molecular size such as 1-octene and octene were used, the activity of Ni-MOF-74-300 was higher than that of Ni/AC-300. On the other hand, substrates with larger

10 molecular size such as trans-stilbene and cyclooctene gave lower
11 reaction rates for Ni-MOF-74-300 compared to Ni/AC-300. The
12 ratio of the reaction rate constant between 1-octene and
13 cyclooctene ($k_{1\text{-octene}}/k = 82.6$) for Ni-MOF-74-300 was 10.6 times
14 higher than that of Ni/AC-300 ($k_{1\text{-octene}}/k = 7.8$). As confirmed by
15 N_2 adsorption/desorption isotherms, the diameter of mesopores
16 in Ni-MOF-74-300 is larger than the size of these molecules,
17 which means the substrate molecules can diffuse into the
18 mesopores to reach the active sites. However, the Ni-MOF-74-
19 300 with Ni NPs@carbon/Ni-MOF-74 core-shell structure enables
20 size-selective hydrogenation for various olefins due to the
21 characteristics of the carbon/Ni-MOF-74 composite shell, which
22 acts as a filter and allows the separation of molecules by their
23 sizes. The size-selectivity in the results of Ni-MOF-74-400 and -
24 600 decreases with increasing heat treatment temperature ($k_{1\text{-}}$
25 $_{\text{octene}}/k = 26.8, 16.8$, respectively) due to exposure of Ni NPs to the
26 outer surface by the decomposition of the composite shell during
27 the heat treatment process, which agrees with the results of XPS
28 spectra without ion gun etching.

29 Catalytic recyclability is one of the critical factors for
30 heterogeneous catalysts. In order to determine the recyclability of
31 the prepared catalyst, a recycling test was carried out in the
32 hydrogenation of 1-octene using the best performing catalyst, Ni-
33 MOF-74-300 (Figure S6). After the fifth cycle, Ni-MOF-74-300
34 maintained its original catalytic activity. Thus, the Ni-MOF-74-300
35 was repeatedly usable at least five times without significant
36 decrease in catalytic activity.

Table 2. Results of hydrogenation of olefins using Ni-MOF-74-T and Ni/AC-300.

Entry	Substrate	Catalyst	Reduction temp. (°C)	Time (h)	Conv. (%)	k (mmol/h)	$k_{1\text{-octene}}/k$
1		Ni-MOF-74-300	200	0.5	97.0	1.94	-
2		Ni-MOF-74-400	200	0.5	49.5	0.99	-
3		Ni-MOF-74-600	200	0.5	42.5	0.85	-
4		Ni/AC-300	400	0.5	46.0	0.92	-
5		Ni-MOF-74-300	200	2.0	55.4	0.28	6.9
6		Ni/AC-300	400	2.0	38.2	0.19	4.8
7		Ni-MOF-74-300	200	2.0	26	0.13	14.9
8		Ni/AC-300	400	2.0	62	0.31	3.0
9		Ni-MOF-74-300	200	2.0	4.7	0.024	82.6
10		Ni-MOF-74-400	200	2.0	7.4	0.037	26.8
11		Ni-MOF-74-600	200	2.0	10.1	0.051	16.8
12		Ni/AC-300	400	2.0	23.5	0.118	7.8

Reaction condition: catalyst (10 mg), olefin (1 mmol), EtOH (10 mL) at 30 °C.

FULL PAPER

Conclusions

In summary, we successfully prepared highly active and size-selective Ni nanocatalysts using Ni-MOF-74 as a precursor via controlled pyrolysis at low temperature. The structural transformations of Ni active sites in Ni-MOF-74 were analyzed in detail by XRD, in situ XAFS, TEM, XPS analyses, etc. Reducing gases such as H₂ and CH₄ produced at around 300 °C accompanied by the decomposition of the structure of Ni-MOF-74 during the heat treatment process reduced the Ni species, resulting in the formation of a Ni metal NPs core and carbon/Ni-MOF-74 composite shell structure. The Ni NPs in Ni-MOF-74-T were reduced at lower temperature than those in conventional Ni/AC-300, which resulted in smaller Ni NPs without excess aggregation. Moreover, the created Ni NPs were in an electronically deficient state owing to the carbonaceous layer surrounding the Ni NPs. In the hydrogenation of 1-octene, Ni-MOF-74-300 showed two times higher activity in comparison with Ni/AC-300, due to the creation of highly dispersed and electron-deficient Ni NPs. In addition, Ni-MOF-74-300 showed not only high activity but also size-selectivity due to the characteristics of the carbonaceous shell derived from the linker of Ni-MOF-74. We believe that this approach can be further extended to various types of MOFs consisting of other metals and/or organic linkers and will find many applications in size-selective reactions such as oxidations, hydrogenations, esterifications and allylations.

Experimental Section

Materials

Ni(NO₃)₂·6H₂O, dimethylformamide (DMF), ethanol, HCl and biphenyl were purchased from Nacal Tesque, Inc. 2,5-Dihydroxyterephthalic acid, 1-octene, 2-octene, trans-stilbene and cyclooctene were obtained from Tokyo Chemical Industry Co., Ltd. Activated carbon (Shirasagi, M644) was obtained from Osaka Gas Chemicals Co., Ltd.

Preparation of Ni-MOF-74-T

Ni-MOF-74 was prepared using the following procedure^[46]. 4.756 g of Ni(NO₃)₂·6H₂O and 0.956 g of 2,5-dihydroxyterephthalic acid were added into 400 mL of a mixture of water, ethanol and DMF with a molar ratio of 1:1:1. After complete dissolution with ultrasonication for 5 min, the solution was transferred into a Teflon bottle and aged at 100 °C for 24 h. The obtained slurry was filtered, washed several times with distilled water and ethanol, and dried at room temperature under vacuum overnight, giving Ni-MOF-74. The as-synthesized Ni-MOF-74 powder was heat-treated at different temperatures for 2 h under 100 mL/min of nitrogen flow. The obtained samples were referred to as Ni-MOF-74-T, in which the T indicates the heat treatment temperature (°C).

Preparation of Ni/AC-300

Ni/AC-300 was employed as a reference and synthesized by the typical impregnation method as follows. 1.0 g of AC (Shirasagi M) and 1.783 g of Ni(NO₃)₂·6H₂O as a Ni source were mixed in 200 mL of water and stirred

for one hour. The solvent was removed under vacuum with a rotary evaporator. After drying at 100 °C overnight, the powder was heat treated at 300 °C for 2 h under N₂ flow (100 mL/min). This material was named Ni/AC-300 and the weight percentage of the Ni species was adjusted to 25.5 wt%, which was calculated from the results of TG/DTA of Ni-MOF-74 (see Supporting Information Figure S1).

Characterization

To measure the Ni amount in Ni-MOF-74, TG/DTA analysis was carried out using a Rigaku thermogravimetry unit, Rigaku Thermo Plus EVO II series high temperature differential thermal balance TG/DTA, with temperature increasing at a ramping rate of 5 °C/min up to 800 °C in air. Powder X-ray diffraction patterns (XRD) were recorded using a Rigaku Ultima IV diffractometer with Cu K α radiation ($\lambda = 1.5406 \text{ \AA}$). N₂ adsorption isotherms were obtained using a BELSORP-max system (microtracBEL Corp.) at -196 °C. The sample was degassed under vacuum for 8 h at 150 °C prior to data collection. X-ray photoelectron spectroscopy (XPS) was performed with a Shimadzu XPS system, ESCA-3400, using the Mg K α line (1253.6 eV). The binding energy was calibrated using the C 1s photoelectronic peak at 285.0 eV. The gas produced during the heat treatment of Ni-MOF-74 was investigated by thermal programmed desorption (TPD) measurements. TPD was performed under an Ar atmosphere using a BELCAT-B system (MicrotracBEL Corp.). Samples (50 mg) were preheated under N₂ gas flow (100 mL/min) for 2 h at 150 °C to eliminate physisorbed water, and allowed to cool to 50 °C. The system was purged with N₂ at 50 °C for 30 min and the measurement was carried out between 100 °C to 800 °C under N₂ flow (100 mL/min) with a pumping rate of 10 °C/min. The produced gases were detected by on-line mass spectrometry. The data for the structural transformation of Ni species was collected using X-ray absorption fine structure analysis (XAFS). The Ni K-edge in situ XAFS and XAFS spectra were recorded at the BL-01 at SPring-8, JASRI, Harima, Japan (Proj. Nos. 2016A1057, 2016A1095, 2016B1104). In both XAFS measurements, a Si(111) double crystal was used to monochromatize the X-rays from the 2.5 GeV electron storage ring. In situ XAFS measurements were performed in transmission mode under 100 mL/min He gas flow under increasing temperature at a ramping rate of 5 °C/min after loading of the as-prepared Ni-MOF-74 sample into the quartz in situ cell. Ni K-edge XAFS spectra were recorded using the fluorescence-field collection technique. The EXAFS data were examined using the EXAFS analysis program, Rigaku EXAFS. Transmission electron microscopy (TEM) images were obtained using a field emission-transmission electron microscope (FE-TEM, Hitachi Hf-2000) operated at 200 kV. Field-emission scanning electron microscopy (FE-SEM) images were taken on a JEOL JSM-6500F with an accelerating voltage of 12 kV.

Catalytic test

To investigate the catalytic performance of the prepared samples, the hydrogenations of olefins were carried out according to the following procedure. 10 mg of each catalyst was placed in a Schlenk tube and reduced by H₂ gas at 200 °C, 400 °C or 500 °C with a flow rate of 20 mL/min prior to the hydrogenation reaction. The mixture of olefins (1 mmol) and biphenyl (0.5 mmol) as an internal standard were added into the reaction tube after pretreatment and kept at 30 °C with magnetic stirring in an oil bath to initiate the reaction. During the reaction, magnetic stirring at 600 rpm was continued. The amount of the product was

FULL PAPER

analyzed by gas chromatography (Shimadzu, GC-14B with Phenomenex ZB-FFAP columns). In the recycling test, 1-octene was employed as a substrate and the catalytic activities were confirmed by checking the conversion of 1-octene after 1 h. The spent catalyst was reused five times by addition of the substrate into the tube and the catalytic activity was calculated from the conversion of 1-octene.

Acknowledgements

The present work was supported by the Grants-in-Aid for Scientific Research (KAKENHI, Nos. 26220911 and 26620194) from the Japan Society for the Promotion of Science (JSPS). This work was also performed under the Cooperative Research Program of "Network Joint Research Center for Materials and Devices. K.N. thanks for the JSPS Research Fellowships for Young Scientists (No. 27.0702) and program for Leading Graduate Schools: "Interactive Materials Science Cadet Program". XAFS spectra were recorded at the beam line 01B1 station in SPring-8, JASRI, Harima, Japan (Proj. Nos. 2016A1057, 2016A1095, 2016B1104).

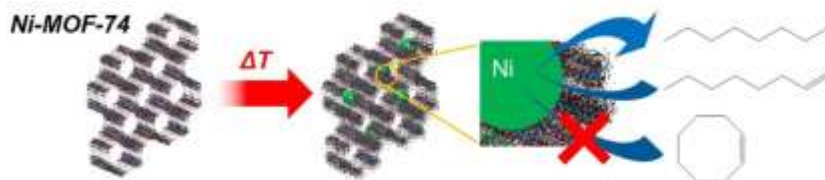
Keywords: Ni-MOF • Ni catalyst • Hydrogenation of olefins • Pyrolysis

- [1] K. Nakatsuka, K. Mori, S. Okada, S. Ikurumi, T. Kamegawa, H. Yamashita, *Chem. Eur. J.* **2014**, *20*, 8348-8354.
- [2] K. Mori, S. Masuda, H. Tanaka, K. Yoshizawa, M. Che, H. Yamashita, *Chem. Commun.* **2017**, *53*, 4677-4680.
- [3] P. Szuromi, *Science* **2015**, *349*, 392-393.
- [4] S.-C. Lin, C.-S. Hsu, S.-Y. Chiu, T.-Y. Liao, H. M. Chen, *J. Am. Chem. Soc.* **2017**, *139*, 2224-2233.
- [5] C. Burda, X. Chen, R. Narayanan, M. A. El-Sayed, *Chem. Rev.* **2005**, *105*, 1025-1102.
- [6] Y. Khalavka, J. Becker, C. Sönnichsen, *J. Am. Chem. Soc.* **2009**, *131*, 1871-1875.
- [7] M. Tamura, D. Yonezawa, T. Oshino, Y. Nakagawa, K. Tomishige, *ACS Catal.* **2017**, *7*, 5103-5111.
- [8] Y. Kuwahara, Y. Fujie, H. Yamashita, *ChemCatChem* **2017**, *9*, 1906-1914.
- [9] S. Bai, Q. Shao, P. Wang, Q. Dai, X. Wang, X. Huang, *J. Am. Chem. Soc.* **2017**, *139*, 6827-6830.
- [10] C. Baldizzone, S. Mezzavilla, H. W. P. Carvalho, J. C. Meier, A. K. Schuppert, M. Heggen, C. Galeano, J.-D. Grunwaldt, F. Schüth, K. J. J. Mayrhofer, *Angew. Chem. Int. Ed.* **2014**, *53*, 14250-14254.
- [11] K. Mori, K. Naka, S. Masuda, K. Miyawaki, H. Yamashita, *ChemCatChem* **2017**, *9*, 3456-3462.
- [12] S. Li, T. Boucheron, A. Tuel, D. Farrusseng, F. Meunier, *Chem. Commun.* **2014**, *50*, 1824-1826.
- [13] S. Li, A. Tuel, D. Laprune, F. Meunier, D. Farrusseng, *Chem. Mater.* **2015**, *27*, 276-282.
- [14] Y. Niu, L. K. Yeung, R. M. Crooks, *J. Am. Chem. Soc.* **2001**, *123*, 6840-6846.
- [15] M. Dincă, J. R. Long, *Angew. Chem. Int. Ed.* **2008**, *47*, 6766-6779.
- [16] S. Kitagawa, R. Kitaura, S.-i. Noro, *Angew. Chem. Int. Ed.* **2004**, *43*, 2334-2375.
- [17] J.-R. Li, Y. Tao, Q. Yu, X.-H. Bu, H. Sakamoto, S. Kitagawa, *Chem. Eur. J.* **2008**, *14*, 2771-2776.
- [18] R. Matsuda, R. Kitaura, S. Kitagawa, Y. Kubota, R. V. Belosludov, T. C. Kobayashi, H. Sakamoto, T. Chiba, M. Takata, Y. Kawazoe, Y. Mita, *Nature* **2005**, *436*, 238-241.
- [19] J. Della Rocca, D. Liu, W. Lin, *Acc. Chem. Res.* **2011**, *44*, 957-968.
- [20] J. An, S. J. Geib, N. L. Rosi, *J. Am. Chem. Soc.* **2009**, *131*, 8376-8377.
- [21] P. Horcajada, C. Serre, M. Vallet-Regí, M. Sebban, F. Taulelle, G. Férey, *Angew. Chem. Int. Ed.* **2006**, *45*, 5974-5978.
- [22] P. Horcajada, C. Serre, G. Maurin, N. A. Ramsahye, F. Balas, M. Vallet-Regí, M. Sebban, F. Taulelle, G. Férey, *J. Am. Chem. Soc.* **2008**, *130*, 6774-6780.
- [23] Z. Xie, L. Ma, K. E. deKrafft, A. Jin, W. Lin, *J. Am. Chem. Soc.* **2010**, *132*, 922-923.
- [24] M. Wen, K. Mori, Y. Kuwahara, H. Yamashita, *ChemCatChem* **2015**, *7*, 3519-3525.
- [25] L. Ma, J. M. Falkowski, C. Abney, W. Lin, *Nat Chem* **2010**, *2*, 838-846.
- [26] L. Ma, C. Abney, W. Lin, *Chem. Soc. Rev.* **2009**, *38*, 1248-1256.
- [27] J. Lee, O. K. Farha, J. Roberts, K. A. Scheidt, S. T. Nguyen, J. T. Hupp, *Chem. Soc. Rev.* **2009**, *38*, 1450-1459.
- [28] Y. Yang, F. Wang, Q. Yang, Y. Hu, H. Yan, Y.-Z. Chen, H. Liu, G. Zhang, J. Lu, H.-L. Jiang, H. Xu, *ACS Appl. Mater. Interfaces* **2014**, *6*, 18163-18171.
- [29] J. Zhuang, L.-Y. Chou, B. T. Sneed, Y. Cao, P. Hu, L. Feng, C.-K. Tsung, *Small* **2015**, *11*, 5551-5555.
- [30] Q. Yang, Q. Xu, S.-H. Yu, H.-L. Jiang, *Angew. Chem. Int. Ed.* **2016**, *55*, 3685-3689.
- [31] P. Hu, J. V. Morabito, C.-K. Tsung, *ACS Catal.* **2014**, *4*, 4409-4419.
- [32] Z. Li, F. Meng, J. Zhang, J. Xie, B. Dai, *Org. Biomol. Chem.* **2016**, *14*, 10861-10865.
- [33] N. V. Maksimchuk, K. A. Kovalenko, V. P. Fedin, O. A. Kholdeeva, *Chem. Commun.* **2012**, *48*, 6812-6814.
- [34] Y. Kuwahara, H. Kango, H. Yamashita, *ACS Sustainable Chem. Eng.* **2017**, *5*, 1141-1152.
- [35] J. Liu, C. Wu, D. Xiao, P. Kopold, L. Gu, P. A. van Aken, J. Maier, Y. Yu, *Small* **2016**, *12*, 2354-2364.
- [36] R. Das, P. Pachfule, R. Banerjee, P. Poddar, *Nanoscale* **2012**, *4*, 591-599.
- [37] X. Li, Y. Fang, X. Lin, M. Tian, X. An, Y. Fu, R. Li, J. Jin, J. Ma, *J. Mater. Chem. A* **2015**, *3*, 17392-17402.
- [38] W. Xia, R. Zou, L. An, D. Xia, S. Guo, *Energy Environ. Sci.* **2015**, *8*, 568-576.
- [39] B. Liu, X. Zhang, H. Shioyama, T. Mukai, T. Sakai, Q. Xu, *J. Power Sources* **2010**, *195*, 857-861.
- [40] A. Banerjee, K. K. Upadhyay, D. Puthusseri, V. Aravindan, S. Madhavi, S. Ogale, *Nanoscale* **2014**, *6*, 4387-4394.
- [41] K. Shen, X. Chen, J. Chen, Y. Li, *ACS Catal.* **2016**, *6*, 5887-5903.
- [42] H. B. Wu, S. Wei, L. Zhang, R. Xu, H. H. Hng, X. W. Lou, *Chem. A Eur. J.* **2013**, *19*, 10804-10808.
- [43] W. Chaikittisilp, K. Ariga, Y. Yamauchi, *J. Mater. Chem. A* **2013**, *1*, 14-19.
- [44] V. Presser, J. McDonough, S.-H. Yeon, Y. Gogotsi, *Energy Environ. Sci.* **2011**, *4*, 3059-3066.
- [45] A. Aijaz, N. Fujiwara, Q. Xu, *J. Am. Chem. Soc.* **2014**, *136*, 6790-6793.
- [46] D. Sun, F. Sun, X. Deng, Z. Li, *Inorg. Chem.* **2015**, *54*, 8639-8643.
- [47] J.-H. Kim, S. H. Kang, K. Zhu, J. Y. Kim, N. R. Neale, A. J. Frank, *Chem. Commun.* **2011**, *47*, 5214-5216.
- [48] N. Dharmaraj, P. Prabu, S. Nagarajan, C. H. Kim, J. H. Park, H. Y. Kim, *Mater. Sci. Eng. B* **2006**, *128*, 111-114.
- [49] T. Sakamoto, K. Asazawa, U. Martinez, B. Halevi, T. Suzuki, S. Arai, D. Matsumura, Y. Nishihata, P. Atanassov, H. Tanaka, *J. Power Sources* **2013**, *234*, 252-259.
- [50] K. Tirez, G. Silversmit, L. Vincze, K. Servaes, C. Vanhoof, M. Mertens, N. Bleux, P. Berghmans, *J. Anal. At. Spectrom.* **2011**, *26*, 517-527.
- [51] C. Guan, Y. Wang, Y. Hu, J. Liu, K. H. Ho, W. Zhao, Z. Fan, Z. Shen, H. Zhang, J. Wang, *J. Mater. Chem. A* **2015**, *3*, 23283-23288.
- [52] S. Chen, M. Xue, Y. Li, Y. Pan, L. Zhu, S. Qiu, *J. Mater. Chem. A* **2015**, *3*, 20145-20152.
- [53] L. Yan, P. Dai, Y. Wang, X. Gu, L. Li, L. Cao, X. Zhao, *ACS Appl. Mater. Interfaces* **2017**, *9*, 11642-11650.
- [54] K. Nakatsuka, T. Yoshii, Y. Kuwahara, K. Mori, H. Yamashita, *Phys. Chem. Chem. Phys.* **2017**, *19*, 4967-4974.
- [55] T. Yoshii, K. Nakatsuka, Y. Kuwahara, K. Mori, Y. Hiromi, *RSC Adv.* **2017**, *7*, 22294-22300.
- [56] T. Yoshii, K. Nakatsuka, Y. Kuwahara, K. Mori, H. Yamashita, *Chem. Lett.* **2017**, *46*, 789-791.

FULL PAPER

Entry for the Table of Contents (Please choose one layout)

FULL PAPER



Ni-MOF-74 heat-treated at 300 °C showed high activity and size-selectivity because of selective formation of Ni NPs covered by MOFs and MOF-derived carbonaceous layer.

Kazuki Nakatsuka, Takeharu Yoshii,
Yasutaka Kuwahara, Kohsuke Mori,
Hiromi Yamashita*

Page No. – Page No.

**Controlled Pyrolysis of Ni-MOF-74 as
a Promising Precursor for the
Creation of Highly Active Ni
Nanocatalysts in Size-selective
Hydrogenation**

Accepted Manuscript